Supporting Information (SI):

Flux Measurements of NO_x, O_3 and O_x: Emission Characteristics, Inventory Validation and Titration Effects

Xiaoxiao Zhang [a], Bin Yuan [a,*], Yibo Huangfu [a], Huizhi Liu [b], Thomas Karl [c], Ming Chang [a], Shiyi Chen [d], Tao Song [e], Jintai Lin [f], Guannan Geng [g], Hongjuan Li [h], and Eran Tas [i]

a. College of Environmental and Climate, Institute for Environmental and Climate Research, Guangdong-Hongkong-Macau Joint Laboratory of Collaborative Innovation for Environmental Quality, Jinan University, 511443 Guangzhou, China
b. Department of Atmospheric Sciences, Yunnan University, Kunming 650091, China
c. Department of Atmospheric and Cryospheric Sciences, University of Innsbruck, Innsbruck, Austria.
d. State Key Joint Laboratory of Environment Simulation and Pollution Control, College of Environmental Sciences and Engineering, Peking University, Beijing 100871, China
e. State Key Laboratory of Atmospheric Boundary Layer Physics and Atmospheric Chemistry, Institute of Atmospheric Physics, Chinese Academy of Sciences, Beijing 100029, China
f. Laboratory for Climate and Ocean-Atmosphere Studies, Department of Atmospheric and Oceanic Sciences, School of Physics, Peking University, Beijing 100871, China.
g. State Key Laboratory of Regional Environment and Sustainability, School of Environment, Tsinghua University, Beijing, 100084, China
h. Beijing Aozuo Ecological Instrument Co., Ltd, Beijing 101160, China.
i. Institute of Environmental Sciences, Soil and Water Department, The Hebrew University of Jerusalem, Israel

*Correspondence: Bin Yuan (byuan@jnu.edu.cn)

Section S1. Details of instrument measurement and correction

At the 102 m platform, two ozone analyzers were installed at the 102 m platform to measure in-situ O_3 flux. A chemiluminescence ozone instrument (FOS-SENSOR, Sextant Technology Ltd.) was used to measure ozone at 10 Hz (FOS-O_3), with an operational flow rate of 3.0 LPM. As the ozone output signals from FOS-O_3 quickly decreased in the time scale of several days due to depletion of the coumarin reagent, an ultraviolet photometry ozone analyzer (model 205, 2B Tech, USA) measuring ozone at 1 Hz with flow at 1.5 LPM was used to correct the response of FOS-O_3. The correction factor is determined as the ratio of 1 Hz O_3 concentrations by the 2B 205 to 10 Hz FOS-O_3 voltage signals every 30 minutes, enabling the derivation of 10 Hz O_3 concentrations (**Fig. S1**).

Other instruments used in this study were housed in a laboratory on ground at the base of the meteorological tower. We deployed two types of NO_2 analyzers to measure NO_x and O_x fluxes, respectively: cavity attenuated phase shift NO_2 analyzer (CAPS, Aerodyne Research, Inc.) and broadband cavity enhanced spectrometer NO_2 analyzer (BBCES). Both instruments are capable of monitoring NO_2 concentrations at 1 Hz. The CAPS instrument applied rapid titration reaction of NO with ozone to measure NO_x ($NO+NO_2$), by delivering high concentrations of ozone generated by 184.5 nm mercury light with a flow of scrubbed and dried air at 10 sccm, whereas the BBCES instrument was used to measure O_x by employing NO as the titration gas (20 sccm, 200 ppm of NO cylinder) (**Fig. S2**). A 100 cm length of 0.90 cm I.D. PFA tubing was served as the ozone + NO reactor for both systems, achieving conversion rate exceeding 96% with 1.5 s of reaction time. The CAPS and BBCES operate at flow rates of 1.2 LPM and 1.5 LPM, respectively. Background measurements were scheduled for 1 min every half an hour for the CAPS instrument, while BBCES background was scheduled every 3 hours for 1 min.

In addition to the CAPS instrument, NO and NO_x were also measured using a custom-built dual-channel chemiluminescence instrument with a time resolution of 1

Hz. In one channel, NO was directly quantified via chemiluminescence with an inlet flow of 0.12 LPM (reactor pressure 210 torr). Another channel (0.44 LPM, 298 torr) reported total NO_x by photolytically converting NO_2 to NO using blue light (395 nm). Concurrently, high-frequency (10 Hz) ozone were also measured using a tunable infrared laser differential absorption spectrometer (TILDAS, Aerodyne Research Inc., USA) operating with sample flow with inlet flow of 1.5 LPM and cell pressure at 40 torr. Volatile organic compounds (VOCs) fluxes were also measured by a proton transfer reaction-mass spectrometer (Vocus PTR-MS, Tofwerk AG, Switzerland).

Sample air from the 102 m platform was transported to ground level via 150 m of 0.90 cm I.D PFA tubing using a high-volume vacuum pump (GAST, Model 1023) with a flow rate of 37 LPM (Huangfu et al., 2024). Extensive experimental tests demonstrating negligible NO_x and O_3 losses within long tubing (Li et al., 2023). Long tubing and high flow rates induce significant pressure drops in the inlet system, which reduce the cell pressure of optical instruments and adversely affect their detection performance (Birks et al., 2018). To address this challenge, we developed a controllable low-pressure calibration system (**Fig. S3**) that enables instrument calibration under simulated low-pressure conditions in the inlet system. During this campaign, CAPS, BBCES and NO_x chemiluminescence instruments were regularly calibrated using this system to ensure data reliability, as shown in **Fig. S4**.

Section S2. Data processing and quality assessment for flux measurements

Before calculation of flux, concentrations of various air pollutants were de-spiked, where spikes were defined as data greater than 3 times the standard deviation of the 10 min running mean. For wind, wind measurements were rotated to ensure that the vertical winds were normal to the shear plane. Since a closed-path system was used in this study, reducing the influence of water vapor, WPL correction was not applied (Aubinet et al., 2012).

Accurate flux measurement requires precise lag-time determination between sampling platform and instrument inlets. Therefore, we used the cumulative covariance

method to determine lag times. By accumulating each covariance curve over an extended period, we were able to accurately determine the lag-time. This approach yielded lag-time measurements for NO_x, O_3, and O_x, as detailed in **Fig. S5**.

In order to obtain more reliable flux data, the averaging period must meet the stationary requirements and fully turbulent. To test the stationarity criterion for eddy covariance calculations, we compared the half-hour flux measurement with the mean of six consecutive 5-min flux (Vickers and Mahrt, 1997). In general, half-hour flux should be rejected when the difference between the covariance of each subinterval and the covariance of the total interval is greater than 30%. In turbulent development tests, the method of flux-variance similarity is utilized to assess the level of turbulence development in the conditions being studied. The flux-variance similarity method has been described in detail in previous work (Striednig et al., 2020). The steady-state test and turbulent development test were consolidated into a comprehensive indicator to filter out the valid flux data. According to this method, 54%, 48%, 50%, 49%, 55%, 51% and 49% of the flux data were valid for CAPS-NO_x, Chemiluminescence-NO, Chemiluminescence-NO_2, Chemiluminescence-NO_x, TILDAS-O_3, FOS-O_3 and BBCES-O_x, respectively.

The concentration data at 1 Hz is utilized in this study, which implies that high-frequencies eddies may not be adequately captured, leading to an unavoidable loss of high-frequency information. Nonetheless, previous research has indicated that at elevated observation sites, the contribution of high-frequency eddies on flux is minimal (Moravek et al., 2013; Raj et al., 2024; Wintjen et al., 2020). As shown in **Fig. S6a**, NO_x, O_3 and O_x have co-spectral densities similar to sensible heat ($w'T'$), decreases in the inertial sub-range with a linear slope (-7/3). The normalized co-spectrum of NO_x, O_3 and O_x (**Fig. S6b**) are also similar to that of $w'T'$ with a maximum in the range 0.002-0.3 Hz. These results indicate that the full range of eddies that contribute to the flux were captured. Comparison of spectral analysis results with fast response instruments with 10 Hz prove that 1 Hz data are sufficient for flux measurements at a height of 102 m. We utilized the spectrum loss module provided by InnFlux for the

evaluation revealed that the high-frequency loss was below 3% (Striednig et al., 2020). Considering the minimal flux losses attributed to both low and high-frequency eddies, we did not correct the flux in this work.

As species can accumulate below the measurement height, this accumulation leads to flux measured by the EC method that are not net flux (Finnigan, 2006). Thus, the storage term must be calculated and subsequently used to correct the measured flux, namely net flux (F_{net}).

$$Flux_{net} = Flux_{EC} + Flux_{Storage} \quad \text{(S1)}$$

The storage term ($F_{Storage}$) was calculated as follows:

$$Flux_{Storage} = \frac{C_{t+1} - C_{t-1}}{T} \times Z_m \quad \text{(S2)}$$

Where C_{t+1} and C_{t-1} are the concentration of species in the before and after flux averaging periods, respectively. T is the total time of in the before and after flux averaging periods. Z_m represent the measurement height. This storage flux is then added to the calculated turbulent flux to obtain the net flux. A cross-instrument comparison of NO_x and O_3 concentrations and fluxes demonstrated good consistency for different measurements (**Fig. S7**). These results demonstrate the validity of the flux observation dataset. We selected NO_x flux from CAPS, O_3 flux from TILDAS, and O_x flux from BBCES as case studies to elucidate the impact of storage term on net flux. **Fig. S8** illustrates that a higher slope and correlation coefficient (R^2) indicate a more significant impacts of storage term on the net flux. Quantitative analysis of the $Flux_{storage}/Flux_{EC}$ ratio also reveals storage term flux contributes substantially during nocturnal-early morning periods. On average, storage fluxes constitute 21%, 41%, and 61% of the net NO_x, O_3, and O_x fluxes, respectively, indicating the storage term of O_3 and O_x contributed significantly to the net flux. Similarly, the fluxes of NO_x, O_3, CH_4, and VOCs measured by other instruments have also been corrected for storage terms.

We further quantified uncertainties in NO_x flux measurements, which primarily originate from three sources (Karl et al., 2018): (a) concentration measurement uncertainty of the NO_x analyzer, (b) systematic errors of measured fluxes, but this error is considered minor (Rantala et al., 2016), and (c) random errors in flux measurements,

calculated according to the method of Langford et al. (2015) and Striednig et al. (2020). For the CAPS system, concentration measurement uncertainty was 5% with random uncertainty of flux measurements at 10%, yielding a flux measurements uncertainty of 15%. The random uncertainty of NO_x fluxes via chemiluminescence NO_x analyzer was estimated to be 12%, and the uncertainty of NO_x concentrations was 8%, resulting in a flux measurements uncertainty of 20%. These values reflect the compounded effects of instrument precision and atmospheric variability on flux quantification.

Section S3. Footprint calculation

The footprint rendering is based on two-dimensional parametrization model (Kljun et al., 2015). The input parameters include the measurement height, standard deviation of the horizontal and vertical wind speed, horizontal wind direction, boundary layer height, surface roughness length and friction velocity. Surface roughness values were taken as 15 m. For each half-hour flux calculation, we calculate the footprint map at the spatial resolution of 10 m and then extract the 10-90% contour. **Fig. S9** shows the average footprint for this campaign with the 90% cumulative contributions to the measured flux. For this campaign the 90% contribution to the measured flux extended as far as 6 km from the tower.

Section S4. Dahmköhler numbers

The Dahmköhler (Da) number is a dimensionless parameter that describes the relative time scale of a transport (τ_{tran}) and chemical reaction (τ_{chem}). Dahmköhler number of NO-NO_2-O_3 triad were calculated as following (Rinne et al., 2012; Vuolo et al., 2017):

$$D_a = \frac{\tau_{tran}}{\tau_{chem}} \quad \text{(S3)}$$

$$\tau_{tran} = \frac{Z}{u_*} \quad \text{(S4)}$$

$$\tau_{chem} = \frac{2}{\sqrt{[{j_{NO2}}^2 + {k_r}^2([O_3]-[NO])^2 + 2*j_{NO2}*k_r([O_3]+[NO]+2*[NO_2])]}} \quad \text{(S5)}$$

Where Z is measurement height, u_* is friction velocity, j_{NO2} represents the photolysis rate and k_3 is the reaction rate constant of NO + O_3.

The O_3 flux Damkoehler ($Da_{flux(O_3)}$) number is refer to (Karl et al., 2023).

$$Da_{flux}(O_3) = \left| Da_{O3} + Da_{NO} \frac{F_{NO}}{F_{O3}} - Da_{NO2} \frac{F_{NO2}}{F_{O3}} \right| \quad \text{(S6)}$$

Da_{O3}, Da_{NO}, and Da_{NO2} represent the Dahmköhler number of O_3, NO, and NO_2, respectively. F_{O3}, F_{NO}, and F_{NO2} represent the O_3, NO, and NO_2 fluxes, respectively. **Fig. S14** shows the *Da* values of NO-NO_2-O_3 triad and O_3 flux. Our campaign measurements revealed an average Da number of 3.3 ± 2.6 for the NO-NO_2-O_3 reaction system, and average flux Da number for O_3 is 2.5 ± 10.4.

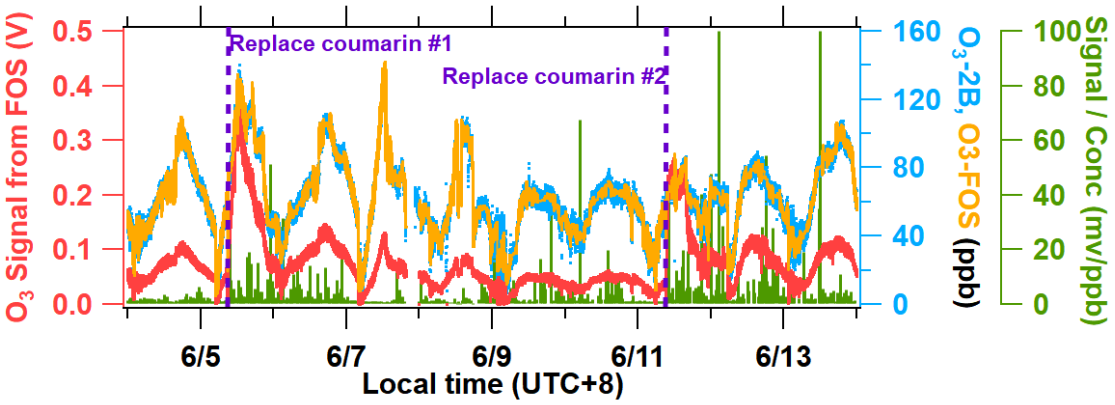


Fig. S1. Measurement data of FOS-O_3 for a selected period to demonstrate the correction process. Every half-hour, the signal to concentration ratio (green line), i.e., the low-frequency ozone concentration (blue line) measured by the 2B 205 analyzer to the high-frequency electrical signal (red line) recorded by the FOS, is calculated. This ratio serves as a correction factor to adjust the high-frequency signal of FOS-O_3, ultimately deriving 10 Hz ozone concentration (yellow line). The two purple dotted lines represent the time for replacing coumarin reagent.

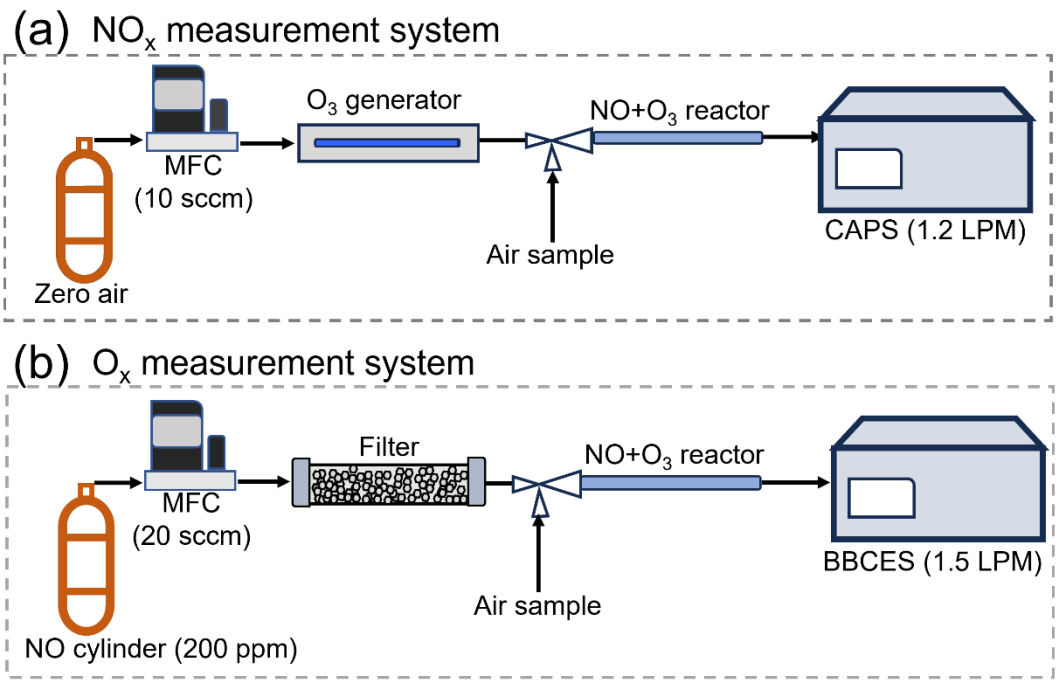


Fig. S2. Schematic of NO_x (a) and O_x (b) measurement systems. The "Filter" unit for the BBCES O_x system is filled with $FeSO_4$, which is used to filter out NO_2. A 100 cm length of 0.90 cm I.D. PFA tubing was served as the NO + O_3 reactor for both systems.

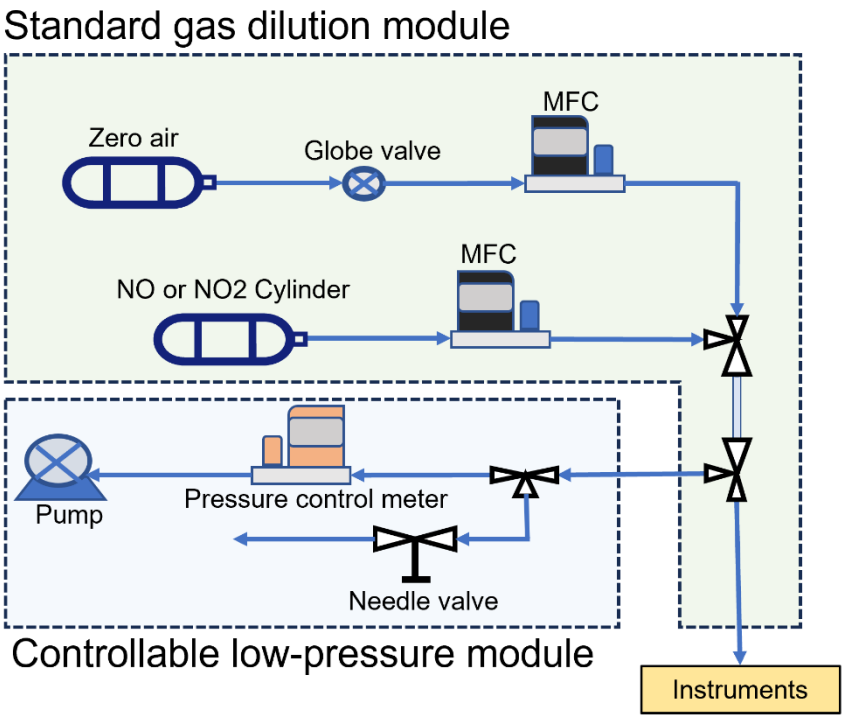
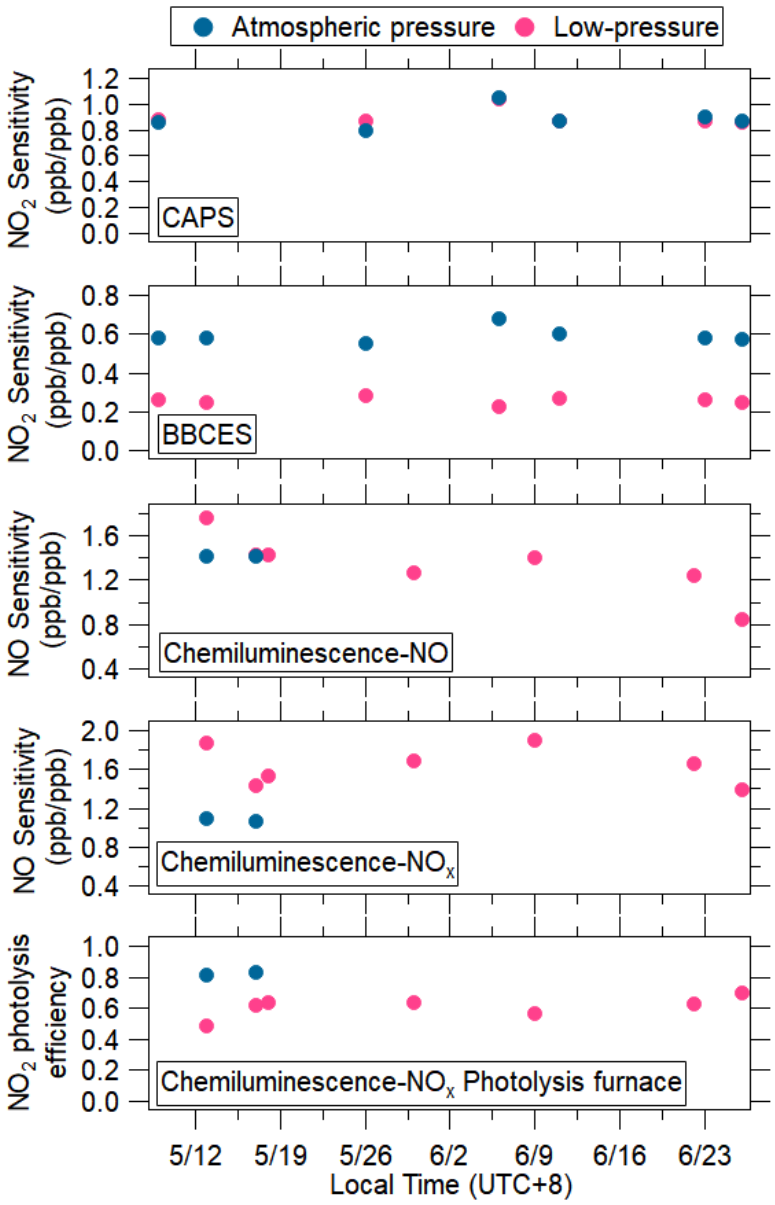


Fig. S3. Schematic of the controllable low-pressure calibration system. The "Standard gas dilution system" supplies calibration gas to instruments, while the "Controllable low-pressure module" generates adjustable low-pressure conditions for gas dilution module.



198

199 **Fig. S4.** Calibration results for CAPS, BBCES, and Chemiluminescence-NO_x under

200 atmospheric-pressure (760 torr) and low-pressure conditions (340 torr), which is the

201 pressure for instrument sampling point of the flux inlet system.

202

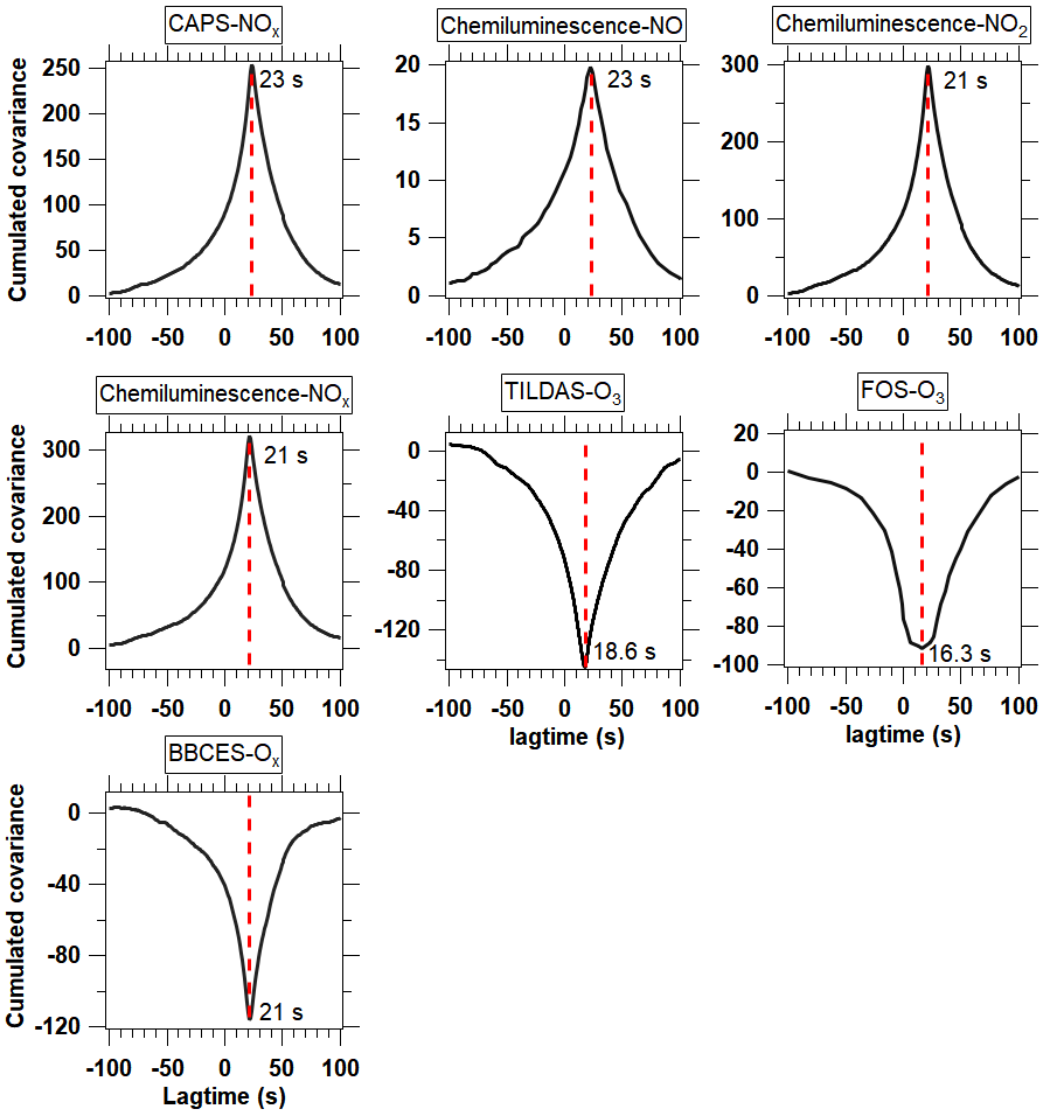
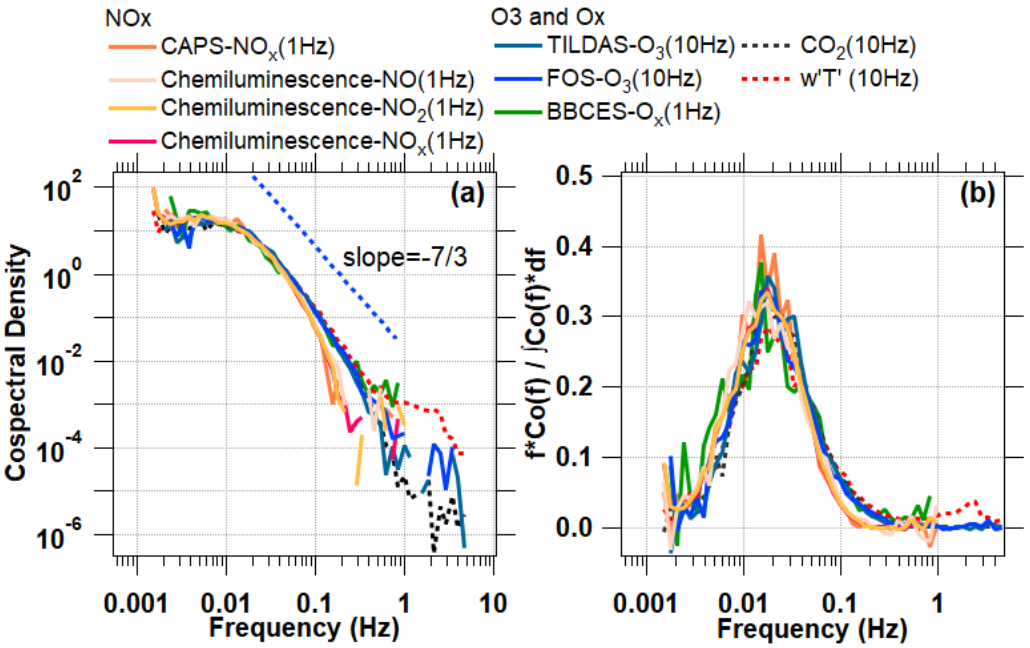


Fig. S5. The determination of lag-times of NO_x (CAPS and Chemiluminescence NO_x analyzer), O_3 (TILDAS and FOS-O_3) and O_x (BBCES) using the cumulative covariance method.

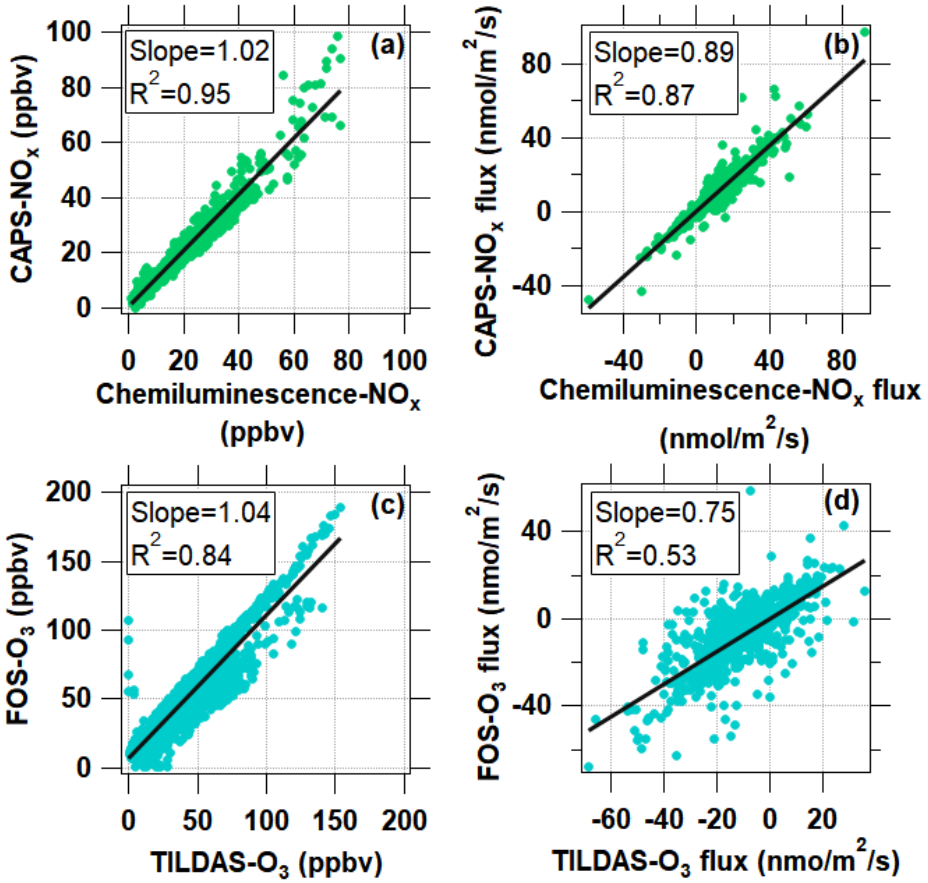


208

209 **Fig. S6.** Co-spectral density (a) and normalized co-spectrum (b) of the NO_x, O_3, O_x,

210 CO_2 and temperature. The blue dashed line in (a) is the reference line with slope of −7/3.

211



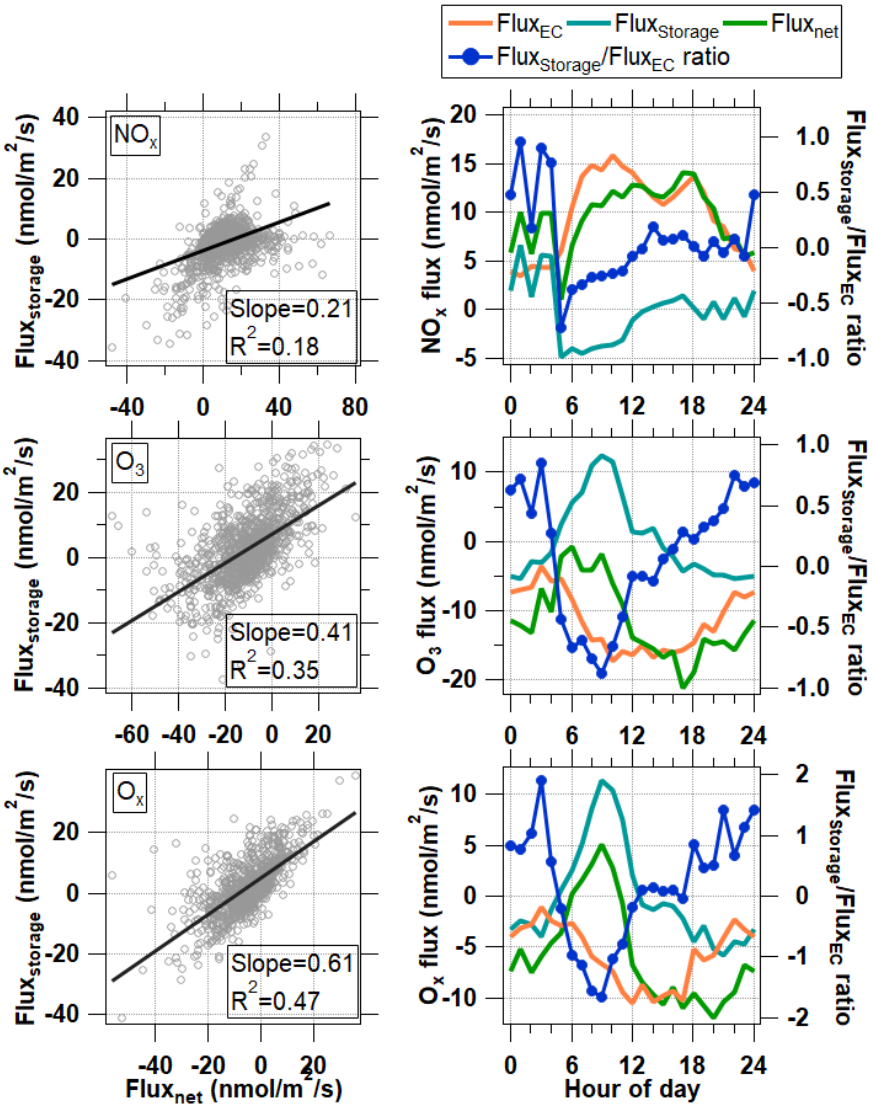
212

213 **Fig. S7.** Comparison of NO_x concentration (a) and flux data (b) between CAPS and the

214 chemiluminescence NO_x analyzer. Comparison of O_3 concentration (c) and flux (d) data

215 between FOS-O_3 and TILDAS.

216



217

218 **Fig. S8.** Scatter plot of NO_x (CAPS), O_3 (TILDAS) and O_x (BBCES) storage flux
219 ($Flux_{storage}$) versus net flux ($Flux_{EC}$ + $Flux_{storage}$) (left panel). Diurnal profiles of EC
220 measured flux, storage flux, net flux and $Flux_{storage}/Flux_{EC}$ ratio (right panel).

221

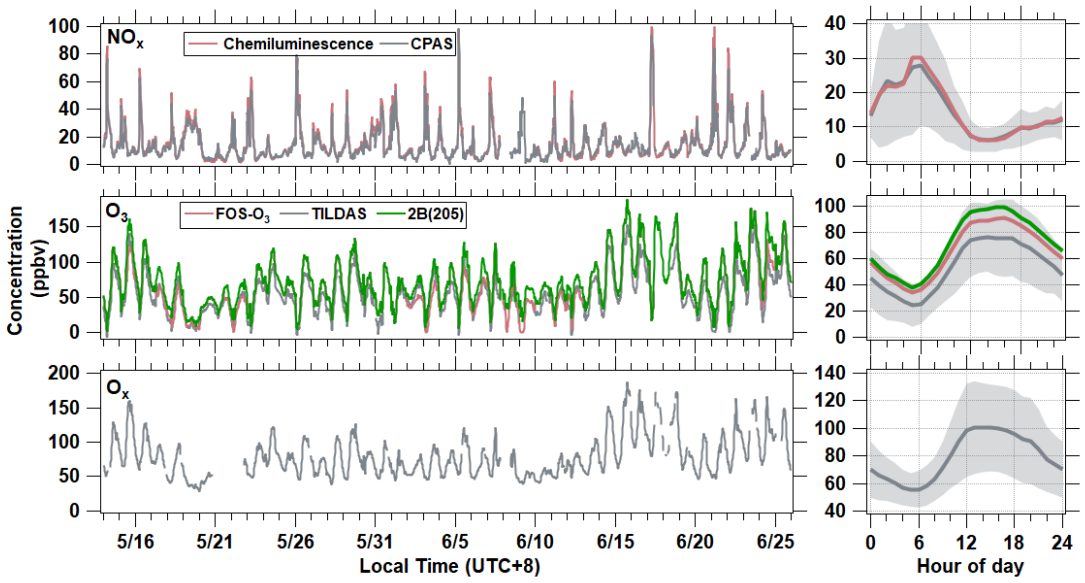


Fig. S9. Time series (left) and diurnal profiles (right) of measured NO_x, O_3 and O_x concentrations.

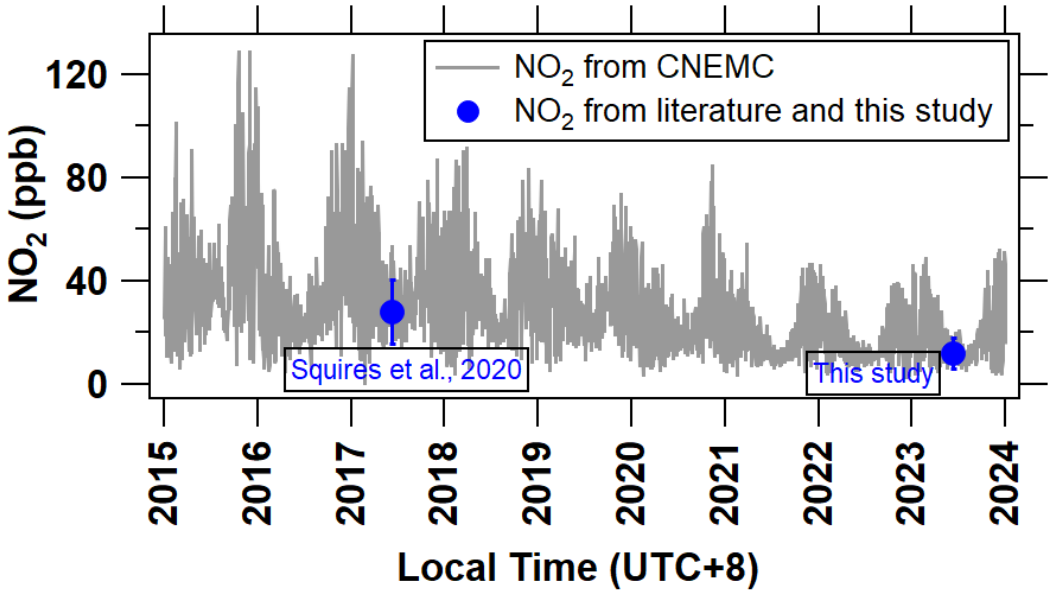
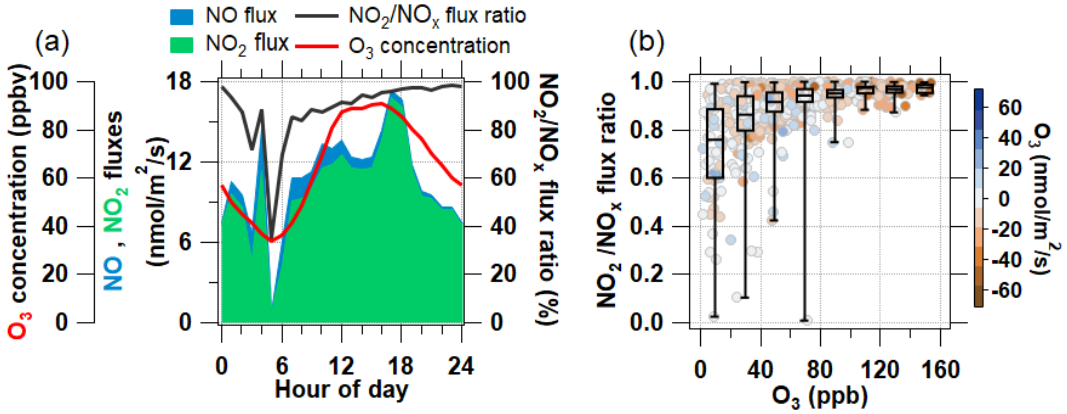


Fig. S10. A comparison of long-term NO_2 daily data from the China National Environmental Monitoring Centre in Beijing (CNEMC, 2023) and NO_2 concentration measured during the 2017 (Squires et al., 2020) and 2023 campaign (this study).



231

232 **Fig. S11.** (a) Diurnal profiles (left) of measured NO and NO_2 fluxes using the
233 chemiluminescence NO_x analyzer at the 102 m platform, as well as the diurnal profile
234 of O_3 concentrations. The black line represents the ratio of NO_2 to NO_x fluxes. (b)
235 NO_2/NO_x flux ratios plotted versus O_3 concentrations, color-code by O_3 flux.

236

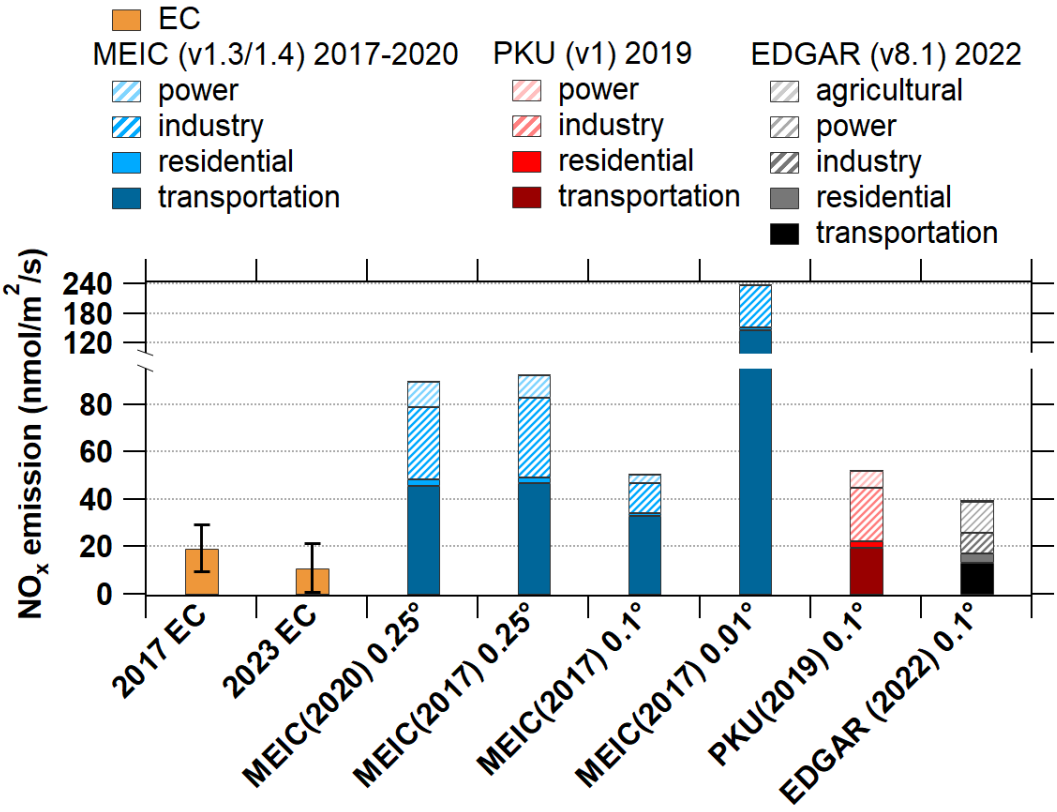


Fig. S12. NO_x emissions quantified via the eddy covariance (EC) method were compared against total emission estimates from three major inventories: MEIC, PKU, and EDGAR. The virtual color bars indicate that inventory may incorrectly allocate emission sources to footprint areas.

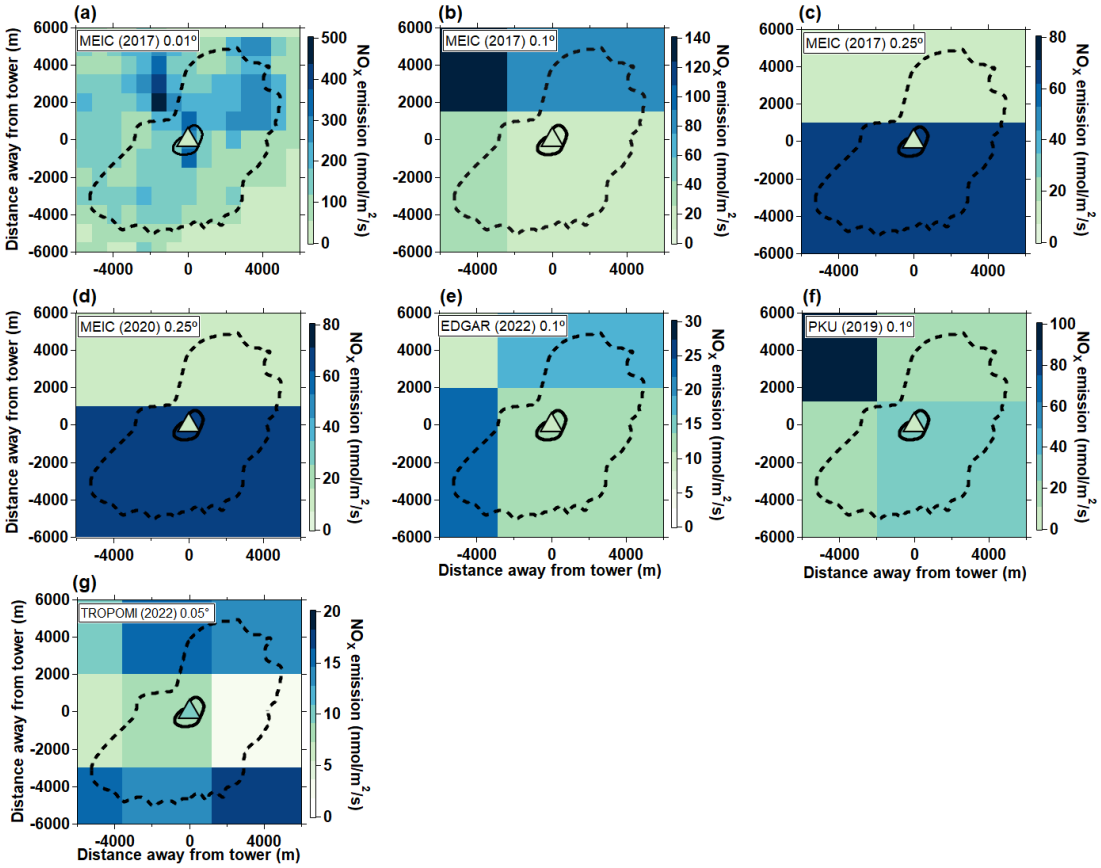


Fig. S13. Spatial distribution of NO_x emissions estimated in inventories (a-f), and retrieved from TROPOMI satellite inversion (g). Note that only emissions from transportation and residential sectors in emission inventories are included. Black solid and dashed lines indicate the calculated footprint encompassing 50% and 90% of the measured flux, respectively. Triangles denote flux tower locations with color-coded by eddy covariance flux measurement in 2023.

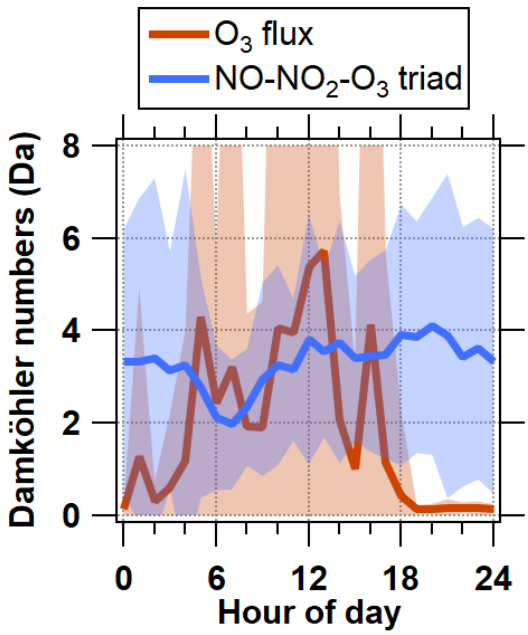


Fig. S14. The Damköhler numbers (Da) for O_3 flux (red line) and the Dahmköhler numbers for NO-NO_2-O_3 (blue line) in this campaign.

References

Aubinet, M., Vesala, T., Papale, D., 2012. Eddy covariance: a practical guide to measurement and data analysis. Springer Science & Business Media.

Birks, J.W., Andersen, P.C., Williford, C.J., Turnipseed, A.A., Strunk, S.E., Ennis, C.A., Mattson, E., 2018. Folded tubular photometer for atmospheric measurements of NO2 and NO. Atmos. Meas. Tech. 11, 2821-2835.

China National Environmental Monitoring Centre (CNEMC). Real-time China Urban Air Quality Release Platform. Last 2023.https://air.cnemc.cn:18007/

Finnigan, J., 2006. The storage term in eddy flux calculations. Agric. For. Meteorol. 136, 108-113.

Huangfu, Y., Yuan, B., He, X., Liu, Z., Zhang, Y., Karl, T., Striednig, M., Ding, Y., Chen, X., Li, H., Zheng, H., Chang, M., Wang, X., Shao, M., 2024. Natural Gas Leakage Ratio Determined from Flux Measurements of Methane in Urban Beijing. Environ. Sci. Technol. Lett. 11, 1025-1031.

Karl, T., Christian, L., Martin, G., Alexander, C., Martin, T., Arellano, J.V.-G.d., David, G., Lenschow, D., 2023. High urban NOx triggers a substantial chemical downward flux of ozone. Sci. Adv. 9, eadd2365

Karl, T., Striednig, M., Graus, M., Hammerle, A., Wohlfahrt, G., 2018. Urban flux measurements reveal a large pool of oxygenated volatile organic compound emissions. Proc. Natl. Acad. Sci. 115, 1186-1191.

Kljun, N., Calanca, P., Rotach, M.W., Schmid, H.P., 2015. A simple two-dimensional parameterisation for Flux Footprint Prediction (FFP). Geosci. Model Dev. 8, 3695-3713.

Langford, B., Acton, W., Ammann, C., Valach, A., Nemitz, E., 2015. Eddy-covariance data with low signal-to-noise ratio: time-lag determination, uncertainties and limit of detection. Atmos. Meas. Tech. 8, 4197-4213.

Li, X.-B., Zhang, C., Liu, A., Yuan, B., Yang, H., Liu, C., Wang, S., Huangfu, Y., Qi, J., Liu, Z., He, X., Song, X., Chen, Y., Peng, Y., Zhang, X., Zheng, E., Yang, L., Yang, Q., Qin, G., Zhou, J., Shao, M., 2023. Assessment of long tubing in measuring atmospheric trace gases: applications on tall towers. Environ. Sci. Atmos. 3, 506-520.

Moravek, A., Trebs, I., Foken, T., 2013. Effect of imprecise lag time and high-frequency attenuation on surface-atmosphere exchange fluxes determined with the relaxed eddy accumulation method. J. GEOPHYS. RES-ATMOS. 118.

Raj, A., Praveen Kumar, B., Jampana, V., Shivaprasad, S., Sureshkumar, N., Rao, E.P.R., Kumar, T.S., Ravichandran, M., 2024. Turbulent characteristics of momentum flux in the marine atmospheric boundary layer of North Bay of Bengal. Sci. Rep. 14.

Rantala, P., Järvi, L., Taipale, R., Laurila, T.K., Patokoski, J., Kajos, M.K., Kurppa, M., Haapanala, S., Siivola, E., Petäjä, T., Ruuskanen, T.M., Rinne, J., 2016. Anthropogenic and biogenic influence on VOC fluxes at an urban background site in Helsinki, Finland. Atmos. Chem. Phys. 16, 7981-8007.

Rinne, J., Markkanen, T., Ruuskanen, T.M., Petäjä, T., Keronen, P., Tang, M.J., Crowley, J.N., Rannik, Ü., Vesala, T., 2012. Effect of chemical degradation on fluxes of reactive compounds – a study with a stochastic Lagrangian transport model. Atmos. Chem. Phys. 12, 4843-4854.

Squires, F.A., Nemitz, E., Langford, B., Wild, O., Drysdale, W.S., Acton, W.J.F., Fu, P., Grimmond, C.S.B., Hamilton, J.F., Hewitt, C.N., Hollaway, M., Kotthaus, S., Lee, J., Metzger, S., Pingintha-Durden, N., Shaw, M., Vaughan, A.R., Wang, X., Wu, R., Zhang, Q., Zhang, Y., 2020.

Measurements of traffic-dominated pollutant emissions in a Chinese megacity. Atmos. Chem. Phys. 20, 8737-8761.

Striednig, M., Graus, M., Märk, T.D., Karl, T.G., 2020. InnFLUX – an open-source code for conventional and disjunct eddy covariance analysis of trace gas measurements: an urban test case. Atmos. Meas. Tech. 13, 1447-1465.

Vickers, Mahrt, 1997. Quality Control and Flux Sampling Problems for Tower and Aircraft Data. J. Atmos. Oceanic Technol. 14, 512–526.

Vuolo, R.M., Loubet, B., Mascher, N., Gueudet, J.-C., Durand, B., Laville, P., Zurfluh, O., Ciuraru, R., Stella, P., Trebs, I., 2017. Nitrogen oxides and ozone fluxes from an oilseed-rape management cycle: the influence of cattle slurry application. Biogeosciences 14, 2225-2244.

Wintjen, P., Ammann, C., Schrader, F., Brümmer, C., 2020. Correcting high-frequency losses of reactive nitrogen flux measurements. Atmos. Meas. Tech. 13, 2923-2948.